Special quasiordered structures: Role of short-range order in the semiconductor alloy (GaN)_{1−x}(ZnO)_{x}

Jian Liu, Maria V. Fernández-Serra, and Philip B. Allen

Special Quasi-ordered Structures: role of short-range order in the semiconductor alloy $(\text{GaN})_{1-x}(\text{ZnO})_x$

Jian Liu,* Maria V. Fernández-Serra, and Philip B. Allen

Department of Physics and Astronomy, Stony Brook University, Stony Brook, NY 11794-3800, United States.

(Dated: January 29, 2016)

This paper studies short-range order (SRO) in the semiconductor alloy $(\text{GaN})_{1-x}(\text{ZnO})_x$. Monte Carlo simulations performed on a density functional theory (DFT)-based cluster expansion model show that the heterovalent alloys exhibit strong SRO because of the energetic preference for the valence-matched nearest-neighbor Ga-N and Zn-O pairs. To represent the SRO-related structural correlations, we introduce the concept of Special Quasi-ordered Structure (SQoS). Subsequent DFT calculations reveal dramatic influence of SRO on the atomic, electronic and vibrational properties of the $(\text{GaN})_{1-x}(\text{ZnO})_x$ alloy. Due to the enhanced statistical presence of the energetically unfavored Zn-N bonds with the strong Zn$3d$-N$2p$ repulsion, the disordered alloys exhibit much larger lattice bowing and band-gap reduction than those of the short-range ordered alloys. Lattice vibrational entropy tilts the alloy toward less SRO.

PACS numbers:

I. INTRODUCTION

Relative to pure end-member materials, the non-isovalent pseudobinary semiconductor alloy $(GaN)_{1-x}(ZnO)_x$ shows improved efficiency as a photocatalyst in splitting water into hydrogen and oxygen under visible light illumination[1]. High efficiency is partly attributed to the band-gap reduction which can be tuned by varying the ZnO content x of the alloy. First-principles calculations show that including short-range order (SRO) affects the band gaps of the heterovalent semiconductor alloys[2,3]. Experiments on different $(GaN)_{1-x}(ZnO)_x$ samples also observe large variation in the band gaps, which could be attributed to the different degrees of SRO introduced in growing the samples. For example, the absorption edge shifts monotonically to longer wavelength with increasing x for samples synthesized by nitridation of nanocrystalline $ZnGa_2O_4$ and ZnO precursors[4], while a minimum gap at $x \sim 0.5$ is found for samples synthesized by mixing of GaN and ZnO powders at high pressure and high temperature[5]. Despite the experimental indication of the presence of SRO, a thorough theoretical understanding is still lacking. An even more challenging question is how the vibrational properties depend on SRO, and how they influence the degree of SRO[6,7]. The effect of lattice vibrations is important for isovalent semiconductor alloy thermodynamic calculations[8]. To our knowledge, to date, there are no published phonon data for $(GaN)_{1-x}(ZnO)_x$. Therefore we perform detailed first-principles investigations to illuminate the role SRO plays on phonons in the $(GaN)_{1-x}(ZnO)_x$ alloy.

Previous theoretical studies assume the $(GaN)_{1-x}(ZnO)_x$ alloy to be completely random[9–11]. The Special Quasirandom Structure (SQS) method[12,13] is often used to construct supercells mimicking random alloys[14]. However, even for isovalent ternary semiconductor alloys, neglecting SRO introduces non-negligible systematic errors[15–18]. For example, the band gaps of $Al_{0.5}Ga_{0.5}As$, $Ga_{0.5}In_{0.5}P$ and $Al_{0.5}In_{0.5}As$ alloys can be reduced by as much as 0.1eV through clustering[16,17]. The electronic properties of wurtzitic $Ga_{1-x}In_xN$ and $Al_{1-x}In_xN$ alloys are also found to be very sensitive to SRO in the cation distribution[18]. For quaternary alloys the sensitivity to SRO is even greater[19,20]. The situation is compounded for the $(GaN)_{1-x}(ZnO)_x$ alloy whose heterovalent nature favors local charge neutrality and therefore valence-matched nearest-neighbor Ga-N and Zn-O pairs. In a previous study on the $(GaN)_{1-x}(ZnO)_x$ alloy[21], referred to hereafter as I, first-principles calculations combined with the cluster expansion method[22–25] and Monte Carlo simulations predicted a large degree of SRO. In constructing the cluster expansion model, the total energy of a specific configuration is calculated in its relaxed structure. Local relaxations of surprisingly large magnitude are found in our subsequent study[26]. The aim of the present study is to construct DFT-affordable supercells whose structural correlations accurately reflect the SRO found by the above approach. The method we use ("special quasi-ordered structure, SQoS") was used in 1998 by Saitta $et\ al$[19] but rarely since then[20]. This method allows us to study with a single DFT calculation, for each x, the statistical average atomic, electronic and vibrational properties of the $(GaN)_{1-x}(ZnO)_x$ alloy. The dependence of structural properties such as bond-length distribution and bond-angle variation upon SRO will be discussed in a separate paper[27].

II. COMPUTATIONAL METHOD

The $(GaN)_{1-x}(ZnO)_x$ alloy was modeled in wurtzite structure with interpenetrating cation and anion hcp sublattices. Ga/Zn can only occupy the cation sublattice, while N/O can only occupy the anion sublattice. A detailed description of the cluster expansion model used in this study can be found in I. Monte Carlo simulations are performed using the $ATAT$ package[28–30] with a $12 \times 12 \times 8$ supercell containing 4608 atoms. For each (x, T), an ensemble of N configurations (labeled by $s = 1, 2, ..., N$) is equilibrated with 1×10^4 MC passes, followed by 1×10^4 MC passes for sampling. The site occupation is denoted by Ising spin σ_i with $\sigma = 1$ denoting Ga/N and $\sigma = -1$ denoting Zn/O respectively. For the structural correlations, the notations are adopted from Ref. 12. The total energy of sample s is expanded in terms of clusters (called "figures" and labeled as $\{k, m\}$). The label $k = 1, 2, ...$ is the number of sites of the cluster. The label $m = 1, 2, ...$ enumerates the distinct cluster geometries, as shown in the inset of Fig. 1. The structural correlation function $\Pi_{k,m}(l, s)$ describes the occupation of the cluster. The label (l, s) indicates that the cluster is located at location l in sample s. For instance, the value of $\Pi_{2,1}(l, s)$ is the spin product $\sigma_i \sigma_j$ for the particular nearest-neighbor pair of sites i and j positioned at location l in sample s. $\overline{\Pi}_{k,m}(s)$ refers to the average of $\Pi_{k,m}(l, s)$ over all locations l in one sample s, and $\langle \overline{\Pi}_{k,m} \rangle$ refers to the average of $\overline{\Pi}_{k,m}(s)$ over the samples equilibrated at a certain (x, T).

The motivation of the SQS approach[12,13] is to approximate the actual alloy with one representative special structure S whose structural correlation functions $\overline{\Pi}_{k,m}(S)$ best match the corresponding ensemble-averaged $\langle \overline{\Pi}_{k,m} \rangle$ of the realistic alloy[12,13]. The original SQS approach reproduces the average structural correlation functions of the $random$ (R) alloy $\overline{\Pi}_{k,m}(S) \sim \langle \overline{\Pi}_{k,m} \rangle_R$[12,13]. We extend the SQS approach to the correlation functions of short-range ordered alloys $\langle \overline{\Pi}_{k,m} \rangle_{SRO}$. We first obtain $\langle \overline{\Pi}_{k,m} \rangle_{SRO}$ by performing Monte Carlo simulations on a DFT-based cluster expansion model. Then we generate numerous site occupancies for a certain composition x and look for the special configuration

S for which the set of $\overline{\Pi}_{k,m}(S)$ is closest to $\langle\overline{\Pi}_{k,m}\rangle_{SRO}$ by minimizing $\sum_{k,m} g_{k,m} D_{k,m} \left[\overline{\Pi}_{k,m}(s) - \langle\overline{\Pi}_{k,m}\rangle_{SRO}\right]^2$, where $D_{k,m}$ is the degeneracy (number of equivalent figures) and $g_{k,m}$ is the assigned weighting factor. Enumeration of all possible configurations is not possible since the number grows exponentially with the number of atoms in the supercell. However, increasing the size of the supercell allows better flexibility of matching structural correlation functions. The conflict is eased by the short-range nature of the structural correlations of the $(GaN)_{1-x}(ZnO)_x$ alloy. The most relevant physical property of the $(GaN)_{1-x}(ZnO)_x$ alloy is the formation energy, which is dominated by the short-range pair structural correlations[21]. We thus assign large weighting factors to the nearest-neighbor $\{2, 1\text{-}2\}$ (meaning $\{2, 1\}$ and $\{2, 2\}$) and next nearest-neighbor $\{2, 3\text{-}6\}$ figures. At each (x, T) we generate 1×10^5 72-atom supercell $(3 \times 3 \times 2)$ candidate structures among which the best-matching structure S is chosen. We emphasize that the obtained structures are not the optimal SQS. However, the contributions to the energetics from longer-range figures $E(s) - \langle E \rangle = \sum_{k,m} D_{k,m} \left[\overline{\Pi}_{k,m}(s) - \langle\overline{\Pi}_{k,m}\rangle_{SRO}\right] \epsilon_{k,m}$ (Eq. (3.1) in Ref. 12) are reasonably small. To avoid confusion, we name the corresponding special structure for the short-range ordered alloy (equilibrated at the experimental synthesis temperature $T = 1,123$K[1]) as SQoS (Special Quasi-ordered Structure), and for the disordered alloy (equilibrated at an unrealistic high temperature $T = 20,000$K) as SQdS (Special Quasi-disordered Structure), in resemblance to the widely used SQS (Special Quasi-random Structure) formalism introduced by Zunger[12,13]. A completely random "SQS" at $x = 0.5$ is also studied for reference. The constructed special structures are provided in supplementary materials[31].

The constructed special structures are fully relaxed with respect to atomic coordinates, volume and shape. Electronic structure calculations are performed using the QUANTUM ESPRESSO package[32] with the PBEsol functional[33]. The pseudopotentials are constructed by means of the projector augmented wave (PAW) method[34,35] with 60 Ry and 240 Ry cutoff energy for plane-wave basis set and charge density respectively. Ga-$3d$ and Zn-$3d$ states are treated explicitly as valence states. The k-point mesh is chosen to be equivalent to a $6 \times 6 \times 4$ mesh for the 4-atom wurtzite unit cell. To speed the structural relaxations, the input lattice parameters are estimated using Vegard's law[36]. Nowadays fairly large supercells (e.g., over 50 atoms) can be handled at the DFT level. For the non-isovalent semiconductor alloys where large structural relaxations are expected, one can greatly improve computational efficiency from a pre-relaxation prior to the expensive DFT total energy and force calculations. We will address the issue of pre-relaxation in a subsequent study[27]. Phonons are calculated using the small displacement method as implemented in the PHON code[37]. For each 72-atom primitive cell, a $2 \times 2 \times 2$ supercell is used while a small displacement of 0.02 $\mathring{A}$ is employed. The structural relaxations and the force constants are calculated using the SIESTA package[38] with the PBE version[39] of the GGA functional. Pseudopotentials for all the atomic species are available from the SIESTA homepage[40], except for Ga a smaller d-orbital cutoff radius is used[41].

GaN and ZnO have a type-II band alignment[11]. The valence band is composed mainly of N-$2p$ states. DFT with LDA or GGA tends to over-delocalize the semicore Zn-d states and consequently over-hybridize the semicore Zn-d states with the N-p states, resulting in an enhancement of the p-d repulsion. The band gap is therefore severely underestimated due to the artificially large p-d repulsion. In this study we add U corrections to the semicore Ga-d and Zn-d states[42]. The on-site Coulomb interaction parameter $U \sim 3.1$eV is determined by a first-principles method adopted in Ref. 43. U is approximated as the screened $atomic$ on-site Coulomb interaction U^{at}/ϵ_∞, where U^{at} is the Coulomb energy cost of placing two electrons at the same site ($U^{at} = E_{at}(d^{n+1}) + E_{at}(d^{n-1}) - 2E_{at}(d^n)$) and ϵ_∞ is the optical (high-frequency) dielectric constant. In this study we take d^9 occupancy as the reference point for d^n and evaluate U^{at} from DFT atomic energies. The optical dielectric constant ϵ_∞ is calculated from linear-response theory[44]. A similar approach of screening the exact-exchange by the dielectric constant is shown to improve significantly the performance of the traditional hybrid functionals[45].

III. RESULTS AND DISCUSSIONS

A. Structural correlation

It was predicted in I that the $(GaN)_{1-x}(ZnO)_x$ alloy is thermodynamically stable over the full range of compositions for $T > 870$K. The $x = 0.5$ alloy orders at low temperature and undergoes a first-order order-disorder transition at $T \approx 870$K. The ground state is an ordered 50%-50% superlattice labeled as $(GaN)_1(ZnO)_1$, where GaN and ZnO double layers stack alternately along the hexagonal c-axis ($P6_3mc$). The formation energy for the $(GaN)_1(ZnO)_1$ superlattice is predicted to be small and negative, indicating weak stability against phase separation. An analogous superlattice structure is also predicted for the $(SiC)_m(AlN)_n$ alloy[2].

Upon alloying, the main effect of SRO is to enhance the statistical presence of the valence-matched nearest-neighbor Ga-N and Zn-O pairs. The ensemble-averaged pair correlation functions $\langle\overline{\Pi}_{2,m}\rangle$ at $x = 0.5$ (Fig. 1) reveal a large degree of SRO. The nearest-neighbor $\langle\overline{\Pi}_{2,1-2}\rangle$ deviate significantly from the null value of the random alloy, while the next

nearest-neighbor $\langle \overline{\Pi}_{2,3-6} \rangle$ are relatively small, comparable with those found in ternary nitride isovalent semiconductor alloys[15]. Longer-range $\langle \overline{\Pi}_{2,7-14} \rangle$ are less important. The long tail of the $\langle \overline{\Pi}_{k,m} \rangle - T$ curve also indicates that SRO persists to high temperature, and therefore complete randomness may not be achievable under common experimental growth conditions. The positive signs of $\langle \overline{\Pi}_{2,1-2} \rangle$ indicate nearest-neighbor preference for the valence-matched Ga-N and Zn-O pairs, while the positive signs of $\langle \overline{\Pi}_{2,3-6} \rangle$ indicate next nearest-neighbor preference for Ga-Ga and Zn-Zn as well as N-N and O-O pairs. The composition dependence of $\langle \overline{\Pi}_{k,m} \rangle$ at $T = 1,123$K is shown in Fig. 2. The deviation of $\langle \overline{\Pi}_{k,m} \rangle$ from that of the random alloy increases upon mixing, and yields the largest deviation at $x = 0.5$, where neglect of SRO is worst. To compare the degree of SRO included in SQoS, SQdS and SQS, we summarize in Table 1 the corresponding structural correlation functions at $x = 0.5$. The 72-atom SQoS, SQdS and SQS accurately reproduce the ensemble-averaged structural correlation functions obtained with a $12 \times 12 \times 8$ supercell. These special structures are expected to yield an accurate description of the atomic, electronic and vibrational properties of the $(\text{GaN})_{1-x}(\text{ZnO})_x$ alloy.
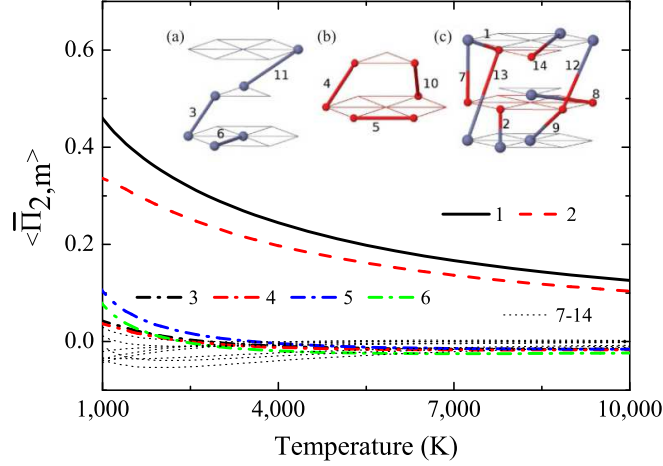

FIG. 1. Ensemble-averaged pair correlation functions $\langle \overline{\Pi}_{2,m} \rangle$ at $x = 0.5$. Definitions of pair figures $\{2, m\}$ can be found in I. $\{2, 1\text{-}2\}$ and $\{2, 3\text{-}6\}$ stand for nearest-neighbor cation-anion pair figures and next nearest-neighbor cation-cation/anion-anion pair figures respectively. Longer-range pair figures $\{2, 7\text{-}14\}$ are shown by dotted lines.
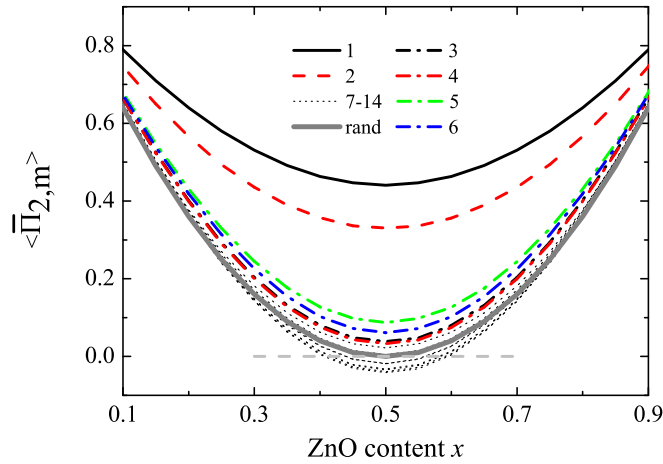

FIG. 2. Ensemble-averaged pair correlation functions $\langle \overline{\Pi}_{2,m} \rangle$ at $T = 1,123$K. The structural correlations for the random alloy $\langle \overline{\Pi}_{k,m} \rangle_R = (2x - 1)^k$ ($k = 2$ for pair correlations) is shown by the solid grey line for comparison.

TABLE I. Pair correlation functions $\overline{\Pi}_{2,m}$ of 72-atom SQoS and SQdS at $x = 0.5$, compared with the target ensemble-averaged pair correlation functions $\langle\overline{\Pi}_{2,m}\rangle$ of 4608-atom supercells at $T = 1,123K$ and $T = 20,000K$ respectively.

	$\overline{\Pi}_{2,m}$-SQoS	$\langle\overline{\Pi}_{2,m}\rangle_{1,123K}$	$\overline{\Pi}_{2,m}$-SQdS	$\langle\overline{\Pi}_{2,m}\rangle_{20,000K}$	$\overline{\Pi}_{2,m}$-SQS
$\{2,1\}$	0.444	0.442	0.074	0.070	0
$\{2,2\}$	0.333	0.333	0.000	0.058	0
$\{2,3\}$	0.037	0.041	-0.037	-0.011	0
$\{2,4\}$	0.037	0.036	0.000	-0.012	0
$\{2,5\}$	0.074	0.089	-0.037	-0.012	0
$\{2,6\}$	0.074	0.063	0.000	-0.016	0

TABLE II. Calculated U^{at}, ϵ_∞ and the corresponding U parameters for GaN and ZnO. Experimental values are shown in parentheses. The PBE version[39] of the GGA functional is used instead of PBEsol in obtaining U^{at}, due to its better treatment of free atoms.

	U^{at} (eV)	ϵ_∞	U (eV)
GaN	18.1	5.9 (5.35)	3.1
ZnO	16.1	5.2 (3.72)	3.1

B. Atomic, Electronic and Vibrational Properties

The calculated U^{at}, ϵ_∞ and U parameters are listed in Table 2. Compared to the experimental values[46], the calculated optical dielectric constant is overestimated due to the band-gap underestimation of DFT. However, since the atomic and electronic structures of GaN and ZnO are not very sensitive to the U parameters, the error in the calculated ϵ_∞ (and also the choice of the reference point for d^n) does not affect the main conclusions drawn in this study. The calculated lattice constants and band gaps are listed in Table 3. DFT-PBEsol calculations accurately reproduce the lattice constants of GaN and ZnO. The band gap of ZnO is more sensitive to the U correction, due to the strong interaction between the high-lying Zn-$3d$ states and the O-$2p$ states. We then perform DFT+U calculations on the SQoS, SQdS and SQS in order to obtain accurate electronic structure properties. For comparison, total energy and force calculations on configurations randomly selected from the $T = 1,123K$ ensembles are also performed within the DFT+U methodology. As shown in Fig. 3, the constructed SQoS accurately represents the ensemble-averaged energetics of the short-range ordered $(GaN)_{1-x}(ZnO)_x$ alloy. The formation energy of SQoS is significantly lower than that of SQdS. The effect of SRO on the energetics grows upon mixing. Even at $T = 20,000K$, the formation energy of SQdS is still considerably lower than that of SQS due to the non-negligible residual SRO.

SRO also plays an important role in determining the structural properties. Fig. 4 compares the lattice constant bowing obtained theoretically and experimentally. Once again, the lattice constants of SQoS accurately reproduce the corresponding ensemble-averaged values. With reduced SRO, the disordered alloy shows an expansion as well as a larger bowing compared to the short-range ordered alloy. The experimentally synthesized samples[4,5] also exhibit moderate bowing, larger than the short-range ordered alloy but smaller than the disordered alloy, indicating the presence of SRO.

Fig. 5 shows the (nearest-neighbor) bond-length distribution of the short-range ordered ($T=1123K$) alloy at $x = 0.5$. In the $(GaN)_{1-x}(ZnO)_x$ alloy, the Ga-N bonds shrink while the Zn-O bonds expand. This unusual bond-length distribution is related to the non-isovalent nature of the alloy. A follow-up study[27] will discuss the prediction and explanation of the bond-length distribution based on the concept of bond valence[47]. For the $(GaN)_{1-x}(ZnO)_x$ alloy,

TABLE III. Calculated lattice constants a and c and band gaps E_g for GaN and ZnO. Experimental values are from Ref. 46.

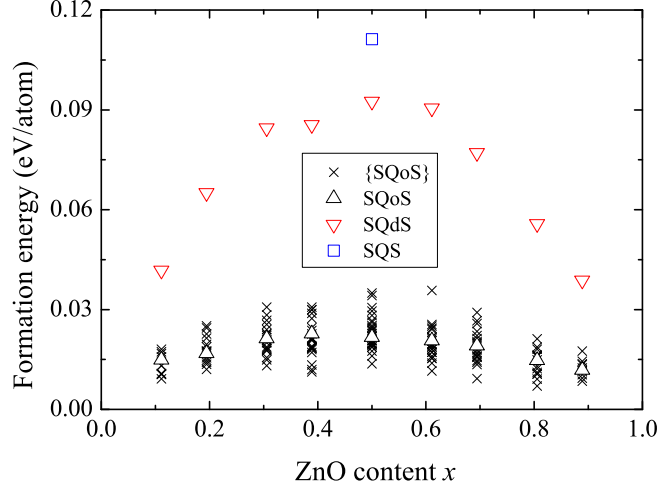|	GaN			ZnO		
	a (Å)	c (Å)	E_g	a (Å)	c (Å)	E_g (eV)
PBEsol	3.182	5.187	1.88	3.225	5.207	0.71
PBEsol+U	3.184	5.189	1.89	3.232	5.213	0.92
Expt.	3.189	5.185	3.51	3.250	5.204	3.44

FIG. 3. DFT-calculated formation energies of SQoS, SQdS and SQS. The crosses are from a set of configurations randomly selected from the $T = 1,123K$ ensemble (labeled {SQoS}).

the Zn-N bond-length distribution has crucial importance since it is related to the band-gap reduction through the Zn3d-N2p repulsion. In the inset of Fig. 5, we show its dependence on the ZnO content. We find that the Zn-N bond-length distribution of the short-range ordered alloy shifts to shorter bonds as the ZnO content increases. Shorter Zn-N bond lengths result in stronger Zn3d-N2p repulsion and therefore significantly push up the top of the valence band.

The bond-angle variation is also unusual, namely N-Ga-N and Ga-N-Ga angles expand while O-Zn-O and Zn-O-Zn angles shrink relative to the ideal tetrahedral angle 109.5°. Fig. 6 shows the variation of bond angles. For example, the Ga-centered bond angle shrinks with increased presence of ligand O atoms. This tendency can also be explained using the concept of bond valence. For Fig. 5 and Fig. 6, see Ref. 27 for a statistically reliable prediction based on the bond valence method.
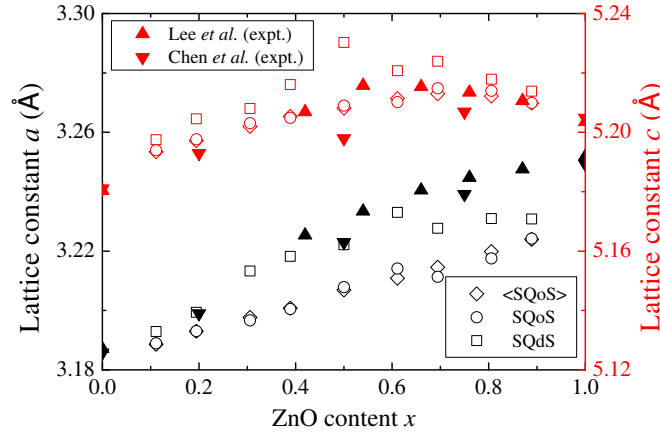

FIG. 4. DFT-calculated lattice constants of SQoS and SQdS. Experimental data (Lee et $al.$ in Ref. 4 and Chen et $al.$ in Ref. 5) are shown as filled triangles. Lattice constants a and c are differentiated by colors. <SQoS> refers to the statistical average of many structures, while SQoS refers to the one special structure.

The atomic and electronic structures of the short-range ordered alloys deviate significantly from those of the disordered alloys. Theoretical atomistic modeling requires explicit inclusion of SRO. Fig. 7 shows the calculated band gaps of SQoS and SQdS. Due to the enhanced statistical presence of the Zn-N bonds, the band gap of the disordered alloy is further reduced relative to that of the short-range ordered alloy. The band-gap reduction is asymmetric. For the disordered alloys the band gap bowing is parabolic, while for the short-range ordered alloys the band gap decreases almost linearly with increasing ZnO in the GaN host. The linear band-gap reduction is maintained even for the unrelaxed short-range ordered alloys, indicating the dominating role of configurational SRO. In Fig. 7 we
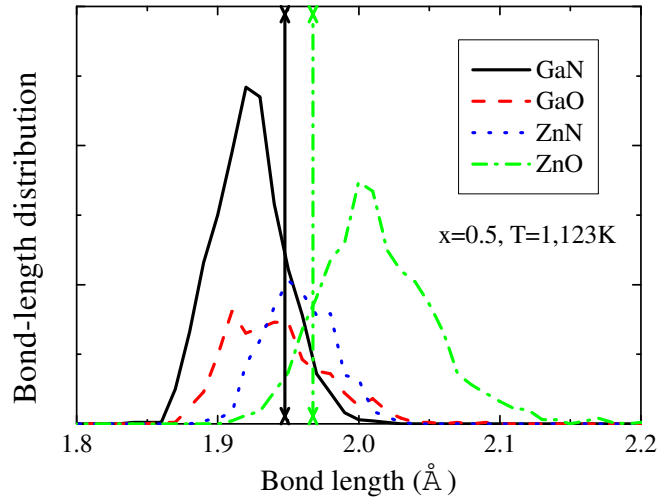
FIG. 5. DFT-calculated bond-length distribution at $T = 1123K$ and $x = 0.5$, with Zn-N bond-length distribution at $T = 1123K$ shown in the inset. Thirty 72-atom structures are selected from the corresponding thermodynamic ensemble. The bin interval is set to 0.01Å (0.02Å in the inset). The vertical lines mark the bond lengths of the corresponding compounds.
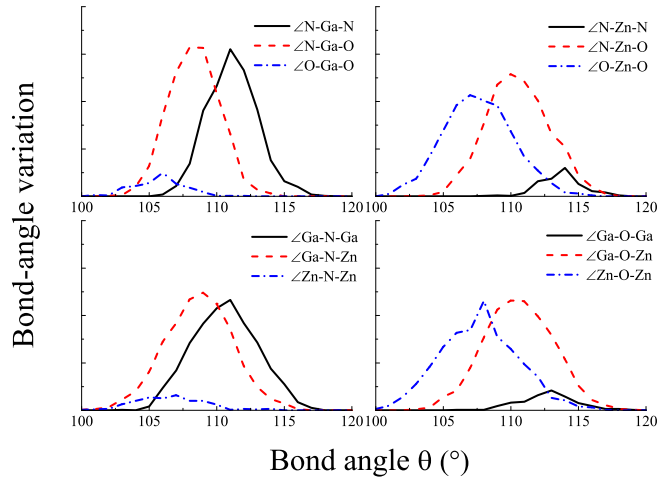

FIG. 6. DFT-calculated bond-angle variation at $(T = 1123K, x = 0.5)$.

also show the linear redshift of the absorption onset with increased ZnO content observed in samples synthesized by nitridation of nanocrystalline $ZnGa_2O_4$ and ZnO precursors[4]. The linearity is a clear indication of the presence of SRO. We also notice that the high-temperature and high-pressure synthesized samples exhibit the minimum gap at $x = 0.5$[5], which is consistent with the parabolic band gap bowing of the random alloy. The parabolic bowing is attributed to the promoted kinetics of mixing at high-temperature and high-pressure. The contrast in the band gap bowing is a clear indication of the importance of SRO. Since the SRO introduced in the sample is related to the synthesis techniques and the growth conditions, one might therefore consider the opportunity of engineering the band gap $E_g(x, T, \Pi)$ via SRO. Fig. 8 compares the projected density of states (PDOS) of SQoS and SQdS at $x = 0.5$. The main contribution to the bottom of the valence bands (approximately -21eV) comes from O-2s states, which are taken as the level of alignment because they are less sensitive to the local chemical environment. The top of the valence band is mainly composed of N-2p states. For the disordered alloy the increased statistical presence of the energetically unfavored Zn-N pairs pushes the band edge upward, resulting in further reduction of the band gap. The N-2p states depend strongly on the local chemical environment. Fig. 9 shows the PDOS of N-2p states with the N atoms surrounded by different numbers of Zn atoms. The N-2p states shift upward (vertical lines in Fig. 9) with increased presence of Zn neighbors.

The effect of lattice vibrations is calculated using the harmonic approximation. The phonon DOS for the SQoS alloys along with those of end-member GaN and ZnO are shown in Fig. 10. Three mechanisms have been suggested
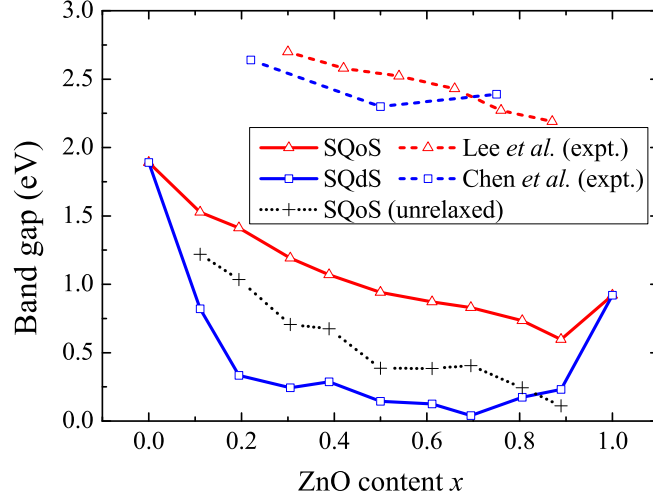
FIG. 7. DFT-calculated band gaps of SQoS and SQdS. Experimental measurements (Lee *et al.* in Ref. 4 and Chen *et al.* in Ref. 5) are also shown for comparison.
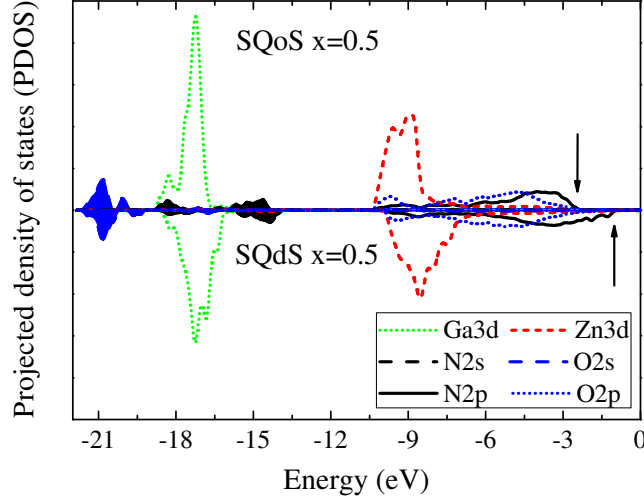

FIG. 8. Projected density of states (PDOS) of the valence bands. The deep-lying anion-s states are shown by the shaded area. The peak positions of O-2s states are taken as the level of alignment. The tops of the valence bands are marked by arrows.

to explain the origin of vibrational entropy differences in alloys[48]: the *bond proportion* effect, the *volume* effect and the *size mismatch* effect. For the $(GaN)_{1-x}(ZnO)_x$ alloy, as the alloy expands with increasing x, the phonon DOS shifts to lower frequencies as the chemical bonds are in general softened. The *volume* effect is magnified by the fact that the "ionic" Zn-O bond is softer than the "covalent" Ga-N bond. Upon disordering, the phonon DOS broadens due to the smeared statistical proportion of different bonds. The low-frequency phonon DOS is well represented by the composition weighted average $(1-x)g_{GaN}(\omega)+xg_{ZnO}(\omega)$. A significant part of the phonon DOS difference (and therefore the vibrational entropy difference) comes from the high-frequency phonons. The effect of SRO is shown for the $x = 0.5$ case. The high-frequency phonon DOS of the SQdS exhibits a much broader spectrum than that of the SQoS. Consequently the phonon mixing entropy of the SQdS is three times larger than that of the SQoS, as is shown in Fig. 11. While the x-dependence of the configurational mixing entropy is symmetric[26], the x-dependence of the phonon mixing entropy is highly asymmetric, indicating that the inclusion of the vibrational free energy into the alloy thermodynamics could alter the shape of the phase diagram. The negative low-T entropy at $x = 0.9$ simply means a phonon stiffening of the acoustic branches in the alloy.
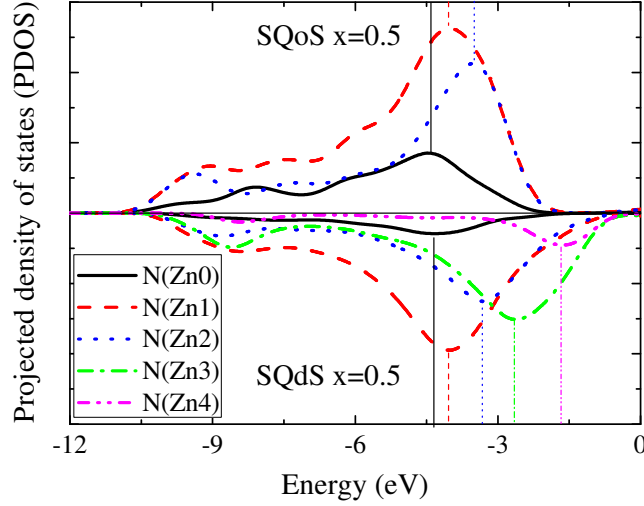
FIG. 9. PDOS of N-2p with N atoms being surrounded by 0, 1, 2, 3 or 4 Zn neighbors. The area under each curve represents the corresponding statistical presence. Vertical lines mark the peak positions and are to aid visualization of the tendency.
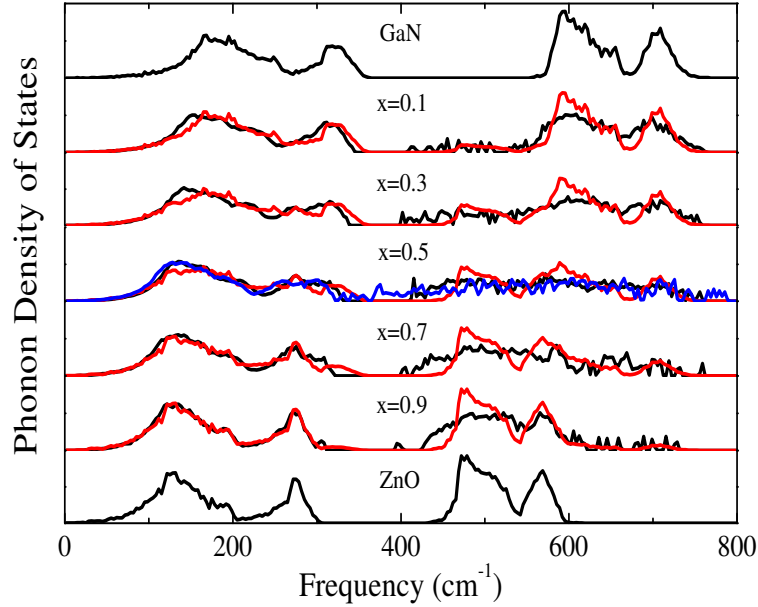

FIG. 10. Phonon DOS for the SQoS (black) ($x = 0.1, 0.3, 0.5, 0.7$ and 0.9) and SQdS (blue) ($x = 0.5$) alloys. The red lines represent the corresponding average of phonon DOS: $(1 - x)g_{\text{GaN}}(\omega) + xg_{\text{ZnO}}(\omega)$.

IV. CONCLUSIONS

The importance of SRO in atomistic modeling schemes such as the SQS approach is often overlooked. For binary metal alloys or isovalent semiconductor alloys, SRO is usually less important. However, for the non-isovalent semiconductor alloys, the valence-matching driving force induces significant SRO. The SQS approach provides a way of approximating the actual alloy with a DFT-affordable supercell. In order to properly compute the non-isovalent alloy, one needs prior knowledge of SRO. In this study the correlated site occupations are provided by Monte Carlo simulations on a DFT-based cluster expansion model. Exhaustive enumeration of all site occupations is avoided due to the SRO in the (GaN)$_{1-x}$(ZnO)$_x$ alloy. We seek to match only the cation-anion nearest-neighbor and the cation-cation/anion-anion next nearest-neighbor correlations. The longer-range correlations are optimized to a lesser extent. Since the short-range nature is generic in the non-isovalency, the construction of SQoS proposed in the present study should also be applicable to other non-isovalent semiconductor alloys. If longer-range correlations come into play, one might apply for example the evolutionary approach[49] in order to efficiently search for the optimal SQoS.
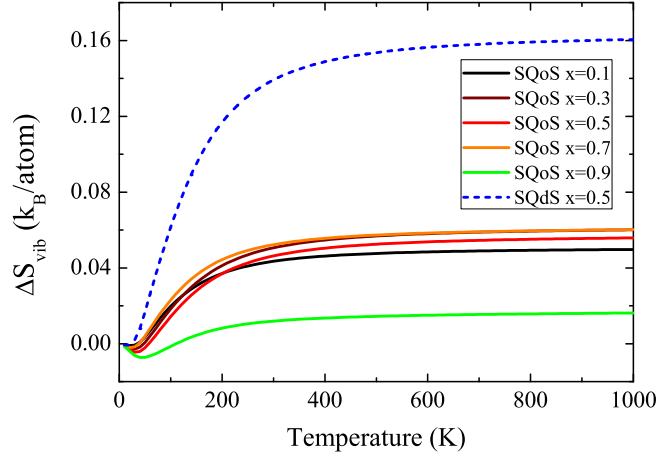
FIG. 11. x-dependence of the phonon mixing entropy $\Delta S_{vib} = S_{vib}(x) - [(1-x)S_{vib}^{\mathrm{GaN}} + xS_{vib}^{\mathrm{ZnO}}]$.

The present study reveals the presence of strong SRO in the $(\mathrm{GaN})_{1-x}(\mathrm{ZnO})_x$ alloy. We construct reliable SQoS and SQdS whose structural correlations reproduce those of the short-range ordered alloys and the disordered alloys respectively. Atomic, electronic and vibrational properties of the short-range ordered alloys deviate significantly from those of the disordered alloys. The short-range ordered alloys experience smaller lattice bowing than the disordered alloys. We offer a tentative explanation in terms of SRO for the discrepancy of the band gaps found in samples synthesized by different methods. SRO inhibits the nearest-neighbor Zn-N pairs, which affects the strength of the Zn3d-N2p repulsion and consequently the top of the valence band. The dependence of the N-2p states on local chemical environment demonstrates the vital role of SRO in accurately describing the $(\mathrm{GaN})_{1-x}(\mathrm{ZnO})_x$ alloy. The phonon DOS is sensitive to the presence of SRO. Disordered alloys have much larger vibrational entropy of mixing than short-range ordered alloys.

* Jian.Liu@stonybrook.edu
[1] K. Maeda, T. Takata, M. Hara, N. Saito, Y. Inoue, H. Kobayashi, and K. Domen, J. Am. Chem. Soc. **127**, 8286 (2005).
[2] B. P. Burton, S. Demers, and A. van de Walle, J. Appl. Phys. **110**, 023507 (2011).
[3] J. Ma, H.-X. Deng, J.-W. Luo, and S.-H. Wei, Phys. Rev. B **90**, 115201 (2014).
[4] K. Lee, B. M. Tienes, M. B. Wilker, K. J. Schnitzenbaumer, and G. Dukovic, Nano Lett. **12**, 3268 (2012).
[5] H. Chen, L. Wang, J. Bai, J. C. Hanson, J. B. Warren, J. T. Muckerman, E. Fujita, and J. A. Rodriguez, J. Phys. Chem. C **114**, 1809 (2010).
[6] A. van de Walle and G. Ceder, Phys. Rev. B **61**, 5972 (2000).
[7] A. Alam, R. K. Chouhan, and A. Mookerjee, Phys. Rev. B **83**, 054201 (2011).
[8] C. K. Gan, Y. P. Feng, and D. J. Srolovitz, Phys. Rev. B **73**, 235214 (2006).
[9] L. L. Jensen, J. T. Muckerman, and M. D. Newton, J. Phys. Chem. C **112**, 3439 (2008).
[10] C. Di Valentin, J. Phys. Chem. C **114**, 7054 (2010).
[11] M. N. Huda, Y. Yan, S.-H. Wei, and M. M. Al-Jassim, Phys. Rev. B **78**, 195204 (2008).
[12] S.-H. Wei, L. G. Ferreira, J. E. Bernard, and A. Zunger, Phys. Rev. B **42**, 9622 (1990).
[13] A. Zunger, S.-H. Wei, L. G. Ferreira, and J. E. Bernard, Phys. Rev. Lett. **65**, 353 (1990).
[14] M. Ferhat and F. Bechstedt, Phys. Rev. B **65**, 075213 (2002).
[15] M. Łopuszyński and J. A. Majewski, Phys. Rev. B **85**, 035211 (2012).
[16] K. A. Mäder and A. Zunger, Appl. Phys. Lett. **64**, 2882 (1994).
[17] K. A. Mäder and A. Zunger, Phys. Rev. B **51**, 10462 (1995).

[18] L. C. de Carvalho, A. Schleife, J. Furthmüller, and F. Bechstedt, Phys. Rev. B **85**, 115121 (2012).

[19] A. M. Saitta, S. de Gironcoli, and S. Baroni, Phys. Rev. Lett. **80**, 4939 (1998).

[20] K. Kim and A. Zunger, Phys. Rev. Lett. **86**, 2609 (2001).

[21] L. Li, J. T. Muckerman, M. S. Hybertsen, and P. B. Allen, Phys. Rev. B **83**, 134202 (2011).

[22] J. Sanchez, F. Ducastelle, and D. Gratias, Physica A **128**, 334 (1984).

[23] J. W. D. Connolly and A. R. Williams, Phys. Rev. B **27**, 5169 (1983).

[24] D. D. Fontaine, in *Solid State Physics*, Vol. 47, edited by H. Ehrenreich and D. Turnbull (Academic Press, 1994) pp. 33 – 176.

[25] A. V. Ruban and I. A. Abrikosov, Rep. Prog. Phys. **71**, 046501 (2008).

[26] J. Liu, L. S. Pedroza, C. Misch, M. V. Fernández-Serra, and P. B. Allen, J. Phys.: Condens. Matter **26**, 274204 (2014).

[27] J. Liu, (submitted) http://arxiv.org/abs/1509.04678.

[28] A. van de Walle and M. Asta, Modell. Simul. Mater. Sci. Eng. **10**, 521 (2002).

[29] A. van de Walle, M. Asta, and G. Ceder, Calphad **26**, 539 (2002).

[30] A. van de Walle and G. Ceder, J. Phase Equilib. **23**, 348 (2002).

[31] See Supplemental Material for the special structures.

[32] P. Giannozzi, S. Baroni, N. Bonini, M. Calandra, R. Car, C. Cavazzoni, D. Ceresoli, G. L. Chiarotti, M. Cococcioni, I. Dabo, A. D. Corso, S. de Gironcoli, S. Fabris, G. Fratesi, R. Gebauer, U. Gerstmann, C. Gougoussis, A. Kokalj, M. Lazzeri, L. Martin-Samos, N. Marzari, F. Mauri, R. Mazzarello, S. Paolini, A. Pasquarello, L. Paulatto, C. Sbraccia, S. Scandolo, G. Sclauzero, A. P. Seitsonen, A. Smogunov, P. Umari, and R. M. Wentzcovitch, J. Phys.: Condens. Matter **21**, 395502 (2009).

[33] J. P. Perdew, A. Ruzsinszky, G. I. Csonka, O. A. Vydrov, G. E. Scuseria, L. A. Constantin, X. Zhou, and K. Burke, Phys. Rev. Lett. **100**, 136406 (2008).

[34] P. E. Blöchl, Phys. Rev. B **50**, 17953 (1994).

[35] A. D. Corso, Comput. Mater. Sci. **95**, 337 (2014).

[36] A. R. Denton and N. W. Ashcroft, Phys. Rev. A **43**, 3161 (1991).

[37] D. Alfè, Comput. Phys. Commun. **180**, 2622 (2009).

[38] J. M. Soler, E. Artacho, J. D. Gale, A. García, J. Junquera, P. Ordejón, and D. Sánchez-Portal, J. Phys.: Condens. Matter **14**, 2745 (2002).

[39] J. P. Perdew, K. Burke, and M. Ernzerhof, Phys. Rev. Lett. **77**, 3865 (1996).

[40] http://www.icmab.es/siesta/.

[41] R. Agrawal and H. D. Espinosa, Nano Lett. **11**, 786 (2011).

[42] S. L. Dudarev, G. A. Botton, S. Y. Savrasov, C. J. Humphreys, and A. P. Sutton, Phys. Rev. B **57**, 1505 (1998).

[43] A. Janotti, D. Segev, and C. G. Van de Walle, Phys. Rev. B **74**, 045202 (2006).

[44] S. Baroni, S. de Gironcoli, A. Dal Corso, and P. Giannozzi, Rev. Mod. Phys. **73**, 515 (2001).

[45] M. A. L. Marques, J. Vidal, M. J. T. Oliveira, L. Reining, and S. Botti, Phys. Rev. B **83**, 035119 (2011).

[46] T. Hanada, in *Oxide and Nitride Semiconductors*, Advances in Materials Research, Vol. 12, edited by T. Yao and S.-K. Hong (Springer Berlin Heidelberg, 2009) pp. 1–19.

[47] I. D. Brown, Chem. Rev. **109**, 6858 (2009).

[48] A. van de Walle and G. Ceder, Rev. Mod. Phys. **74**, 11 (2002).

[49] D. Lerch, O. Wieckhorst, G. L. W. Hart, R. W. Forcade, and S. Müller, Modelling Simul. Mater. Sci. Eng. **17**, 055003 (2009).